Neutral atom imaging of solar wind interaction with the Earth and Venus

M.-C. Fok, T. E. Moore, and M. R. Collier
NASA Goddard Space Flight Center, Greenbelt, Maryland, USA

T. Tanaka
Department of Earth and Planetary Science, Kyushu University, Fukuoka, Japan

Received 18 June 2003; revised 24 September 2003; accepted 9 October 2003; published 13 January 2004.

[1] Observations from the Low-Energy Neutral Atom (LENA) imager on the Imager for Magnetopause-to-Aurora Global Exploration (IMAGE) mission have emerged as a promising new tool for studying the solar wind interaction with the terrestrial magnetosphere. Strong LENA emissions are seen from the magnetosheath during magnetic storms, especially during high solar wind dynamic pressure when the magnetopause is strongly compressed and the magnetosheath penetrates deeply into the exosphere. Venus, unlike the Earth, has no intrinsic magnetic field, so the solar wind penetrates deeply and interacts directly with its upper atmosphere. Energy transfer processes enhance atomic escape and thus play a potentially important role in the evolution of the atmosphere. We have performed simulations of the solar wind interaction with both Earth and Venus and compared the results to LENA observations at the Earth. Low-energy neutral atom emissions from Venus are calculated based on the global MHD model of Tanaka. We found the simulated energetic neutral atom (ENA) emissions from Venus magnetosheath are comparable or greater than for the Earth. The Venus ionopause is clearly seen in the modeled oxygen ENA images. This simulation work demonstrates the feasibility of remotely sensing the Venusian solar wind interaction and resultant atmospheric escape using fast neutral atom imaging. *INDEX TERMS:* 2780 Magnetospheric Physics: Solar wind interactions with unmagnetized bodies; 2784 Magnetospheric Physics: Solar wind/magnetosphere interactions; 2151 Interplanetary Physics: Neutral particles; 2756 Magnetospheric Physics: Planetary magnetospheres (5443, 5737, 6030); 2728 Magnetospheric Physics: Magnetosheath; *KEYWORDS:* neutral atom imaging, solar wind/magnetosphere interactions, solar wind/Venus interactions, atmospheric escape

Citation: Fok, M.-C., T. E. Moore, M. R. Collier, and T. Tanaka (2004), Neutral atom imaging of solar wind interaction with the Earth and Venus, *J. Geophys. Res.*, *109*, A01206, doi:10.1029/2003JA010094.

1. Introduction

[2] The Imager for Magnetopause to Aurora Global Exploration (IMAGE) satellite was launched on 25 March 2000. IMAGE carries neutral atom, ultraviolet, and radio plasma imaging instruments to study the global responses of the terrestrial magnetosphere and ionosphere to the changes in the solar wind input [*Burch*, 2000]. The Low-Energy Neutral Atom (LENA) imager on IMAGE was designed to monitor the ion outflow from the ionosphere and to image the fast neutrals in the solar wind or from the interstellar medium [*Moore et al.*, 2000]. In 3 years of data analysis and modeling efforts, LENA has produced a number of science achievements. By comparing the LENA fluxes with changes in the solar wind during the event on 24 June 2000, *Fuselier et al.* [2002] found prompt responses of ionospheric outflow to solar wind pressure pulses. Based on observations from LENA and other neutral atom-related data sets, *Collier et al.* [2003] suggested that there exists a secondary stream of interstellar neutral atoms entering the heliosphere from somewhere around the galactic center. LENA has also been found to respond to the neutral atoms formed by magnetosheath interactions with the geocorona during periods of high solar wind pressure [*Collier et al.*, 2001; *Moore et al.*, 2003]. Structures of the magetosheath and the cusp are revealed in LENA images. LENA imaging has thus emerged as a new tool for studying the magnetospheric responses to the solar wind variations.

[3] Venus has almost no intrinsic magnetic field to shield itself from the solar wind. The solar wind thus directly interacts with the planetary ionosphere and the atmosphere. A shock is formed when the supersonic solar wind encounters the planet. The shocked solar wind slows down as it approaches the planet. The slowed and compressed flow results in magnetic field buildup and a magnetic layer or barrier is formed that separates plasmas from the solar wind and the ionosphere. This boundary also defines the planetary

0148-0227/04/2003JA010094$09.00

ionopause. The position of the ionopause varies with the solar wind condition and solar cycle. Usually, it extends to higher altitude during solar maximum [*Phillips and McComas*, 1991], when there is greater ionospheric production by solar EUV. Owing to the close contact with resultant energy transfer, interaction of Venus with the solar wind may be important in the escape and evolution of the planetary atmosphere. Ion-electron pairs are produced in the exosphere by photoionization and impact ionization. Atmospheric neutrals are converted to ions by charge exchange. In both cases, new ions formed outside the ionopause are picked up by the solar wind immediately. Some of these pickup ions are accelerated to energies above the escape energy and lost from the planet. On the other hand, some pickup ions may return back to the atmosphere owing to their gyro-motion. They collide with the neutral atoms, some of which attain escape velocity in this "sputtering" process.

[4] In the past there have been quite a few missions to Venus [*Jastrow and Rasool*, 1969; *Dunne*, 1974; *Colin and Hunten*, 1977], but none of them have been equipped with neutral atom imaging instruments to probe the plasma environment of the planet. Current knowledge on the bow shock, magnetosheath, ionosphere and atmosphere escape is from in situ measurements only. The global dynamics and variability of these features are poorly understood and subject to improved understanding if they can be remotely sensed. Since solar wind plasma penetrates into the upper atmosphere, strong energetic neutral atom (ENA) emissions from Venus are expected. The successful ENA imaging technique applied on Earth should also be applicable to image the plasma environment of Venus.

[5] In this paper, we first show a case study of the event on 31 March 2001, when the IMAGE LENA Imager observed strong emissions from the magnetosheath, during a high-pressure solar wind event. By comparing the observations with ENA images simulated from the H^+ distributions of a magnetohydrodynamic (MHD) model, we found the enhanced ENA fluxes are the result of magnetosheath ions charge exchanging with exosphere hydrogen. Using the tools we developed for the Earth study, we then performed similar ENA emission calculations for Venus, based on the plasma distributions generated from the solar wind-Venus interaction model of *Tanaka and Murawski* [1997]. While the solar wind interaction with Earth is visible in neutral atoms mainly when the solar wind pressure is unusually high, the Venus solar wind interaction is shown to be a strong source of fast neutral atoms for most solar wind conditions. This work represents the first study on Venus ENA emissions, and the simulation demonstrates a method for globally monitoring the Venusian solar wind interaction and the resultant atmospheric escape.

2. IMAGE LENA Observations on 31 March 2001

[6] On 31 March 2001 at about 0055 UT, a dense and strongly magnetized interplanetary shock hit the Earth's magnetosphere resulting in strong geomagnetic activity that lasted over a day (minimum Dst = −358 nT). The solar wind density as measured by the Wind spacecraft reached a peak in excess of 100 cm^{-3} near 0440 UT, well over an order of magnitude higher than typical values. Between the time of the shock and 0800 UT, LANL-94 at geosynchronous orbit and close to noon local time observed the magnetopause and bow shock move inside 6.6 Earth radii (R_E) several times. Figure 1 shows the LENA data on 31 March 2001. The top panel is the LENA spin-time spectrogram from 0000 to 0800 UT. The dashed line is the spin phase that contains the Sun direction and the two solid lines mark the Earth's limb. The IMAGE satellite was near the apogee at this time. As shown in the figure, strong fluxes are seen between the Sun direction and the Earth (zero spin azimuth) from 0400 to 0600 UT. As an example, the bottom left panel of Figure 1 plots the spin phase distribution at 0420 UT, the time is marked by a yellow bar in the spin-time spectrogram. The strong and spiky signal corresponds to ENAs directly coming from the solar wind. The smooth and diffused emissions have a peak at ∼50° spin azimuth. The solar wind flux from 0330 to 0600 UT from the ACE spacecraft is plotted in the bottom right panel. Two major peaks in the solar wind flux (or solar wind dynamic pressure) in this period of time are seen at 0420 and 0450 UT and a minimum in between at 0435 UT. The LENA fluxes display the same time variation signature as the solar wind flux, indicating the close relation between low-energy atom emission and the solar wind dynamic pressure.

[7] In order to understand the source and location of the strong LENA emissions during periods of high solar wind flux, we have performed an ENA simulation for this event. The plasma environment is predicted by the MHD model developed at the University of Michigan [*Groth et al.*, 2000], running at the NASA Goddard Space Flight Center Community Coordinated Modeling Center. ENAs are produced when energetic ions charge exchange with the H exosphere. The newly formed ENAs retain approximately the energies and directions of the parent ions. The ENA fluxes are calculated by line of sight integration along each viewing direction:

$$j_{\mathrm{ENA}} = \int j_{\mathrm{ion}} \sigma_{\mathrm{H,ion}} n_{\mathrm{H}} \, dl \tag{1}$$

where j_{ion} is the H^+ differential flux, n_{H} is neutral H density, and $\sigma_{\mathrm{H,ion}}$ is charge exchange cross section of H^+ ions with neutral H. The integration is from the position of IMAGE to the edge of the emission volume, which is confined in 4–12 R_E radial distances to exclude the ENAs generated from the high-energy ring current. The model of *Rairden et al.* [1986] is used for the geocoronal density. It can be seen in equation (1) that strong ENA fluxes are produced where ion flux and/or neutral density are high along the line of sight integration. The simulated LENA fluxes for the 31 March 2001 event are shown in the left-top panel of Figure 2. As shown in the figure, the simulation reproduces the strong fluxes observed at 0400–0600 UT (top panel, Figure 1). Peak emissions occur at times of solar wind pressure enhancements. In the right panel of Figure 2, the simulated image at 0420 UT is depicted. On the image, L shells of 3 and 6.6 are indicated by white circles. Dipole field lines at four magnetic local times are also shown. As shown in the image, peak emissions are seen at ∼50° and 96° spin angles, consistent with the LENA spin profile shown in Figure 1 (bottom left panel). The bottom left panel of Figure 2 shows the physical space these two look directions pass through.

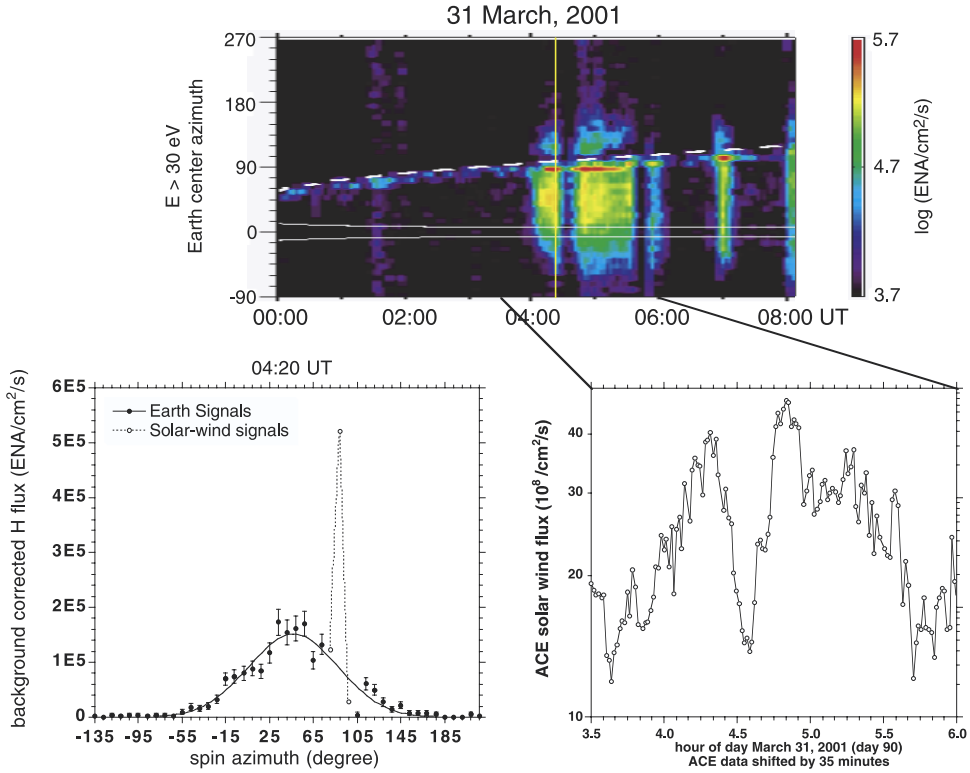

Figure 1. (top) IMAGE LENA spin-time spectrogram on 31 March 2001. (bottom left) Spin profile of LENA fluxes at 0420 UT; the time is marked by a yellow bar in the top panel. (bottom right) ACE solar flux data (shifted by 35 min) from 0330 to 0600 UT.

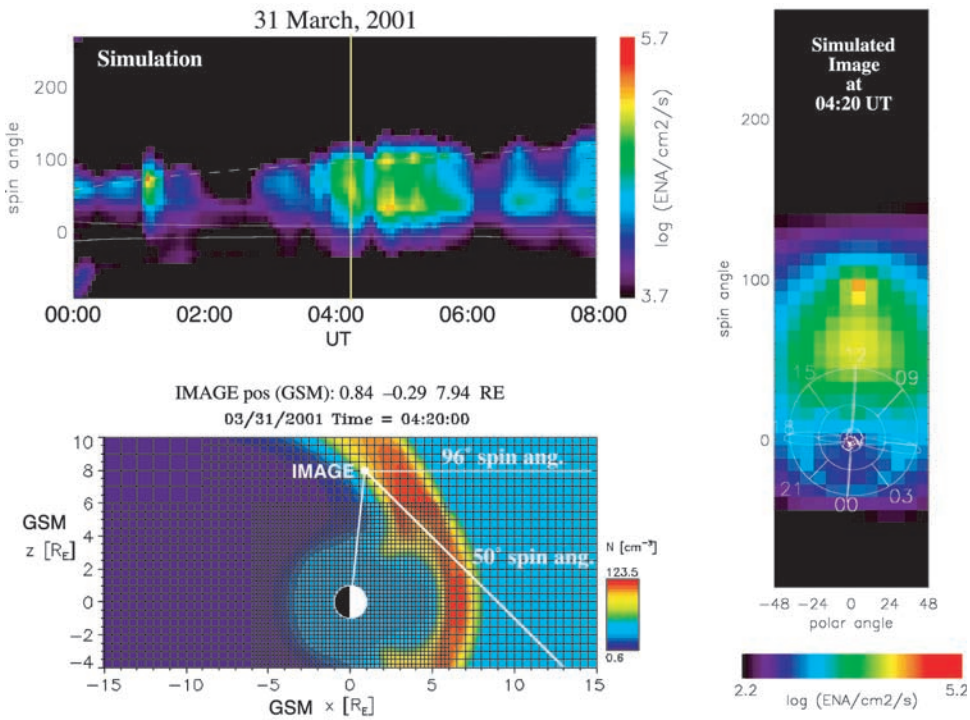

Figure 2. LENA simulation of the 31 March 2001 event. Left panels from top to bottom show simulated LENA fluxes from 0000 to 0800 UT and MHD H^+ number density at 0420 UT. Also shown in the H^+ plot are IMAGE positions with two look directions. Right panel shows simulated LENA image at 0420 UT. The white circles are $L = 3$ and 6.6.

It can be seen that the MHD model predicts a very compressed magnetosphere at this time, with magnetopause standoff distance at about 5.5 R_E. The shocked magnetosheath plasmas penetrate deep into the region of high geocoronal hydrogen density, resulting in strong charge exchange interactions and consequentially strong but diffuse ENA emissions seen, with a peak around 50° azimuth. In contrast, a strong but localized emission is seen in the solar wind flow direction at 96° azimuth. This narrow signal is from solar wind hydrogen ion charge exchange outside the bow shock, where solar wind Mach number is high. The relatively small thermal spread of the solar wind confines the signature to a narrow range of look directions. This strong, highly moderated emission in the solar wind flow direction is observed only when the bow shock is close to the Earth, where geocoronal density is appreciably high. The weaker and continuous signals in the solar wind direction on the LENA summary plot are neutral solar wind generated to a large degree by charge exchange source at larger distances from Earth. This nonexospheric neutral solar wind is not included in the calculation of the simulated fluxes.

3. Venus Low Energy Neutral Atom Simulation

[8] As we have shown in the previous section, strong ENA emissions are produced between the Sun and Earth directions when solar wind and magetosheath plasmas come close and overlap with the geocoronal hydrogen. On Venus, because there is essentially no intrinsic magnetic field, the bow shock is formed deep within the planetary atmosphere. Strong ENA emissions are expected even under nominal solar wind conditions. We have carried out simulations to predict the low-energy neutral atom emissions on Venus and evaluated the fluxes a spacecraft would see if it is equipped with a LENA imager. In addition to hydrogen ENAs, we also estimate the intensities of oxygen ENAs. O^+ is a major species of the Venus ionosphere, which is embedded with the neutral atmosphere. Thus significant oxygen ENA emissions are anticipated if O^+ is heated or accelerated to escape velocity. In the Venus low-energy neutral atom simulation, the Venus International Reference Atmosphere (VIRA) model [*Keating et al.*, 1985] is used for the neutral composition and temperatures in the upper atmosphere. The VIRA model gives H and O densities at altitudes below 3500 km. Neutral densities at high altitudes are fitted by the Chamberlain distribution with exobase density and temperature specified at 250 km altitude. Figure 3 shows the altitude profiles of neutral H (upper panel) and O (lower panel) of the VIRA model. The temperatures and densities at the exobase are also indicated in the figure. It can be seen that there are thermal and hot components in both the neutral H and O. *Cravens et al.* [1980] found that the major sources of hot H are charge exchange of energetic H^+ with atomic H and O and exothermic reaction involving O^+ and H_2. On the other hand, the main contribution of hot oxygen is the dissociative recombination of O_2^+ ions [*Nagy et al.*, 1990]. The hot H and O have relatively large-scale heights and are responsible for the ENA emissions at high altitudes.

[9] The Venus plasma distributions are given by a two-component, three-dimensional MHD model of *Tanaka and Murawski* [1997]. The impinging solar wind is represented by H^+ ions, and the ionosphere is assumed to consist of only

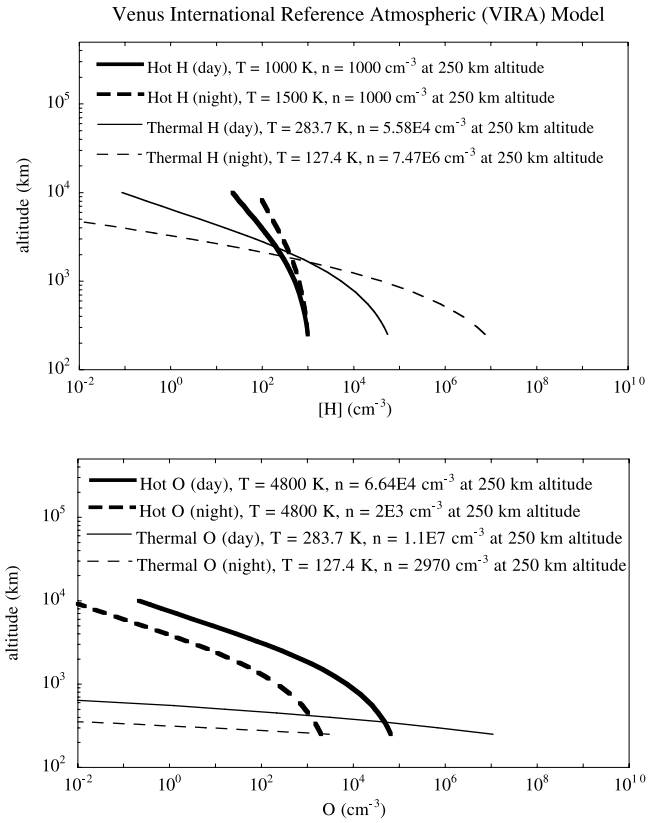

Figure 3. VIRA model. Top panel shows thermal and hot H altitude profiles. Bottom panel shows thermal and hot O altitude profiles.

O^+ ions, which are produced by photoionization of atomic oxygen in the upper atmosphere and by charge exchange with CO_2^+ ions. The two species are assumed to flow with the same velocity and have the same temperature as well. Figure 4 plots the simulated H^+ and O^+ number densities from the MHD model. Spatial coordinates are for a coordinate system with Z-axis perpendicular to the ecliptic. The X-Y plane is the ecliptic plane and the X-axis is pointing antisunward. Atypically of the real solar wind, the IMF Bx = By = 0, Bz = 14 nT, Vsw = 400 km/s and Nsw = 14 cm^{-3}. As seen in Figure 4, the formation of bow shock, magnetotail, and ionopause are reproduced in the MHD model. The bow shock is located very close to the planet at noon at ~2400 km altitude, overlapping with the dense upper atmosphere whose scale height is ~1000 km. The O^+ ions in the ionosphere are picked up by the solar wind flow and form a tail-like bulge on the nightside. The wing-like structures at the equator at solar zenith angle of ~140° are results of magnetic field draping.

[10] With both the neutral and plasma environments being specified, the Venus ENA fluxes are obtained, similarly to equation (1), by:

$$j_{\mathrm{ENA}} = \int j_{\mathrm{ion}}\left(\sigma_{\mathrm{H,ion}} n_{\mathrm{H}} + \sigma_{\mathrm{O,ion}} n_{\mathrm{O}}\right) dl \qquad (2)$$

As shown in the equation, contributions from ion charge exchange with the neutral O is also included in the ENA

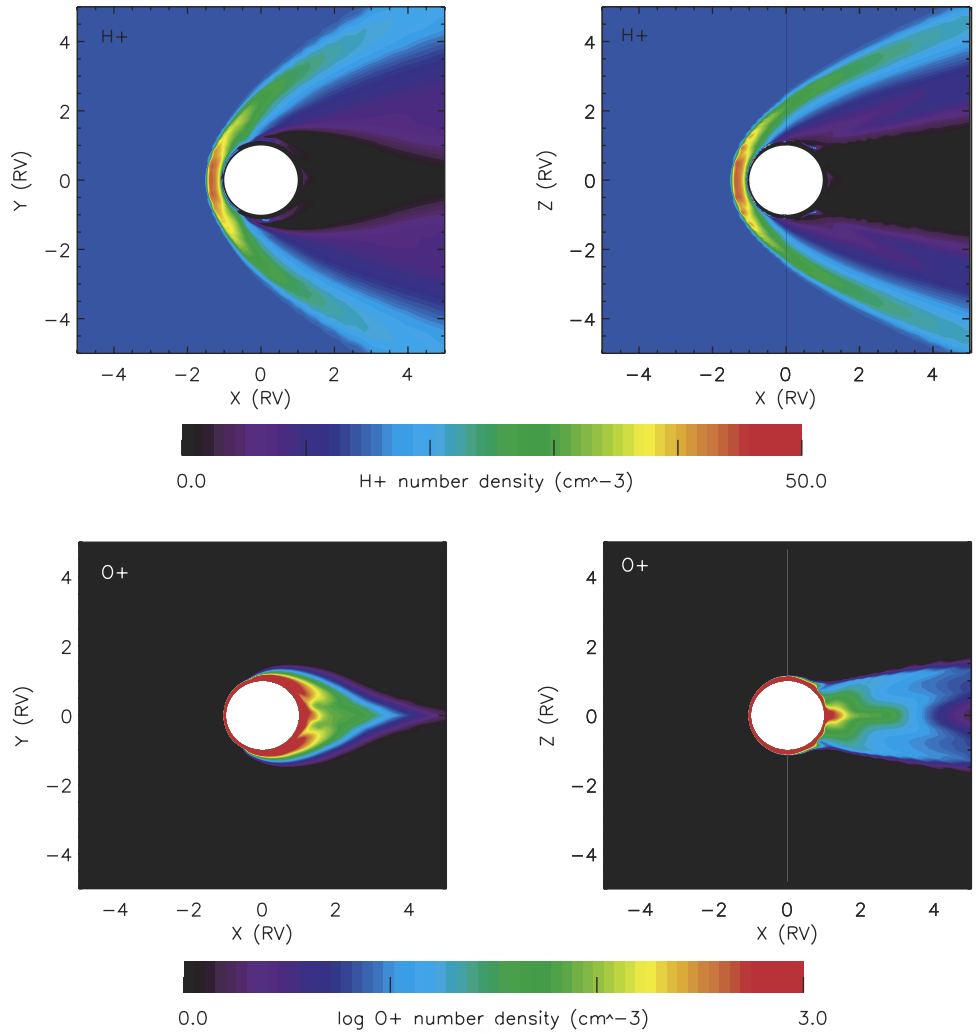

Figure 4. Simulated H^+ (upper panels) and O^+ (lower panels) number densities on Venus in the X-Y (left) and X-Z (right) planes.

calculations. The emission volume is assumed to be from 250 km to 2 Venus radii (R_V) altitudes. We have simulated the ENA emissions along the orbit of a virtual spacecraft, which orbits around Venus in a high-inclination polar orbit with perigee at 500 km and apogee at 5000 km altitude. The orbit period is 2.5 hours. Figure 5 shows the calculated ENA H fluxes from 2 eV to 10 keV at two vantage points: in noon-midnight meridian at high latitude (left) and dawn-dusk plane near the equator (right). The white circle is the limb of the planet and the blue circle is the equator. The Sun direction, north pole, and the ram direction are also indicated in the figure. In the polar view (left panel), strong H emissions are seen in the Sun direction and from the dayside magnetosheath where solar wind protons are hot and dense, and relatively isotropic in angular distribution. The general feature and intensity are similar to those of the Earth (right panel, Figure 2), except the strong sheath emission is located near the limb of Venus rather than at $\sim$4 R_E in the case of the Earth. The localized peak flux in the solar direction are ENAs produced outside the bow shock, where solar wind flow is unidirectional, similar to the situation observed and simulated at Earth. The right panel is a view from dawn. The Sun is on the right but beyond the instrument field of view. This image provides an excellent side-view of the magnetosheath and bow shock. The location of the bow shock at the subsolar point and the latitudinal extent and other characteristics of the magnetosheath can be inferred from this image.

[11] Two simulated oxygen ENA images are shown in Figure 6, viewing from noon-midnight (left) and dawn-dusk (right) meridians. In the midnight view (left panel), O emissions are mainly from the low-altitude ionosphere. The sharp dropout of ENA flux above the planet's limb highlights the ionopause. The magnetotail does not show up in this image partly owing to the vantage point and partly to the relatively low temperature predicted by the MHD model. However, stronger emissions seen on the nightside (negative azimuth) indicate a relatively extended ionosphere in this local time sector. The right panel is a view from dusk at high latitude. Again the Sun is on the right and outside the field of view. The oxygen emissions are low because only fluxes in the energy range of 30 to 680 eV are plotted. We restrict our attention to these energies in order to exclude emissions around the ram direction and strong

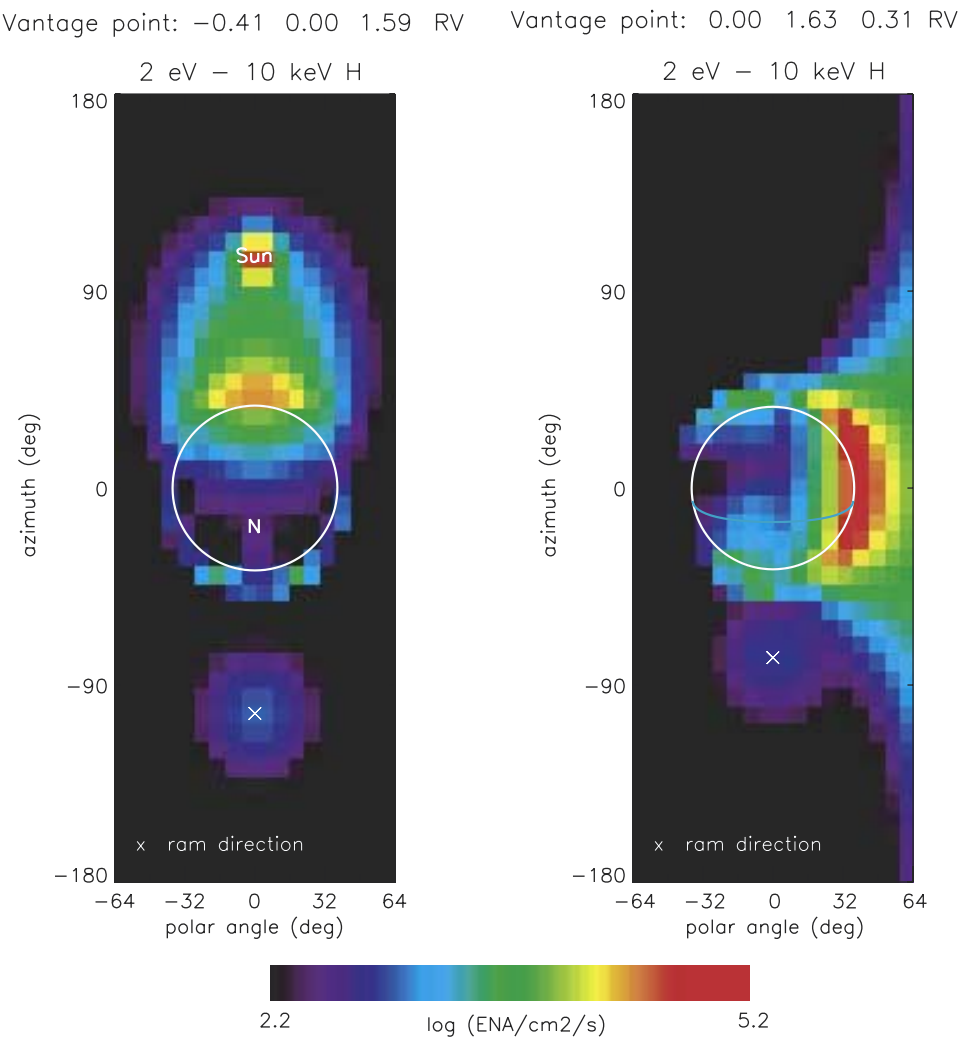

Figure 5. Simulated Venus hydrogen ENA images from vantage points in the noon-midnight meridian (left) and dawn-dusk plane (right). The white circle is the limb of the planet and the blue circle is the equator. In the right panel, Sun is on the right but beyond the instrument field of view.

fluxes from the dayside, such that the faint emission from the nightside ionosphere bulge can be seen in the image. This nightside signature is coming from the ionosphere wing in the premidnight sector (lower left panel, Figure 3). Even though the O^+ density is high there, ENA emissions are low owing to low temperature in that region.

[12] Another noticeable feature in the simulated images in Figures 5 and 6 is the emission around the spacecraft ram direction. The spacecraft velocity is ~5.3 km/s in all images shown in Figures 5 and 6. These ram signals are ambient exospheric H and O that are rammed into the instrument by the spacecraft motion. From the thermal spreads and intensities of these enhancements, the in situ neutral temperatures and densities can be deduced. In case of the O ram signal (Figure 6, left panel), we fit the ENA flux around the ram direction with a Gaussian distribution: flux = a $\exp(-\theta^2/\sigma^2)$, where θ is the polar angle. The thermal velocity (V_{th}) of the ambient exospheric neutrals is obtained by: $\tan\sigma = V_{th}/V_{sc}$, where V_{sc} is spacecraft velocity. The O temperature calculated by this method is 4754 K, which agrees well with the real hot O temperature (4800 K) with only ~1% of error. On the other hand, the ambient density can be estimated by the total ram flux divided by the spacecraft velocity.

4. Oxygen Escape Rate on Venus

[13] O^+ escape flux is a measure of solar wind energy transfer to the Venus ionosphere. As we have mentioned above, O^+ ions on Venus are picked up by the solar wind and energized. Energetic O^+ with velocities greater than escape velocity may be lost from the planet. A portion of the ionospheric O^+ ions may also undergo charge exchange reaction and become ENAs. These oxygen atoms are no longer confined by magnetic and electric fields and immediately fly on direct paths with velocities before collision. Losses due to charge exchange may be important in the total oxygen escape. We have calculated the Venus oxygen escape rate as a result of charge exchange processes. Figure 7 depicts the simulated escape rate per solid angle in all directions from the planet. There is a strong day-night asymmetry, with low escape rate on the dayside and high rate on the nightside. Most of the ENAs created on the dayside will precipitate into the atmosphere rather than fly

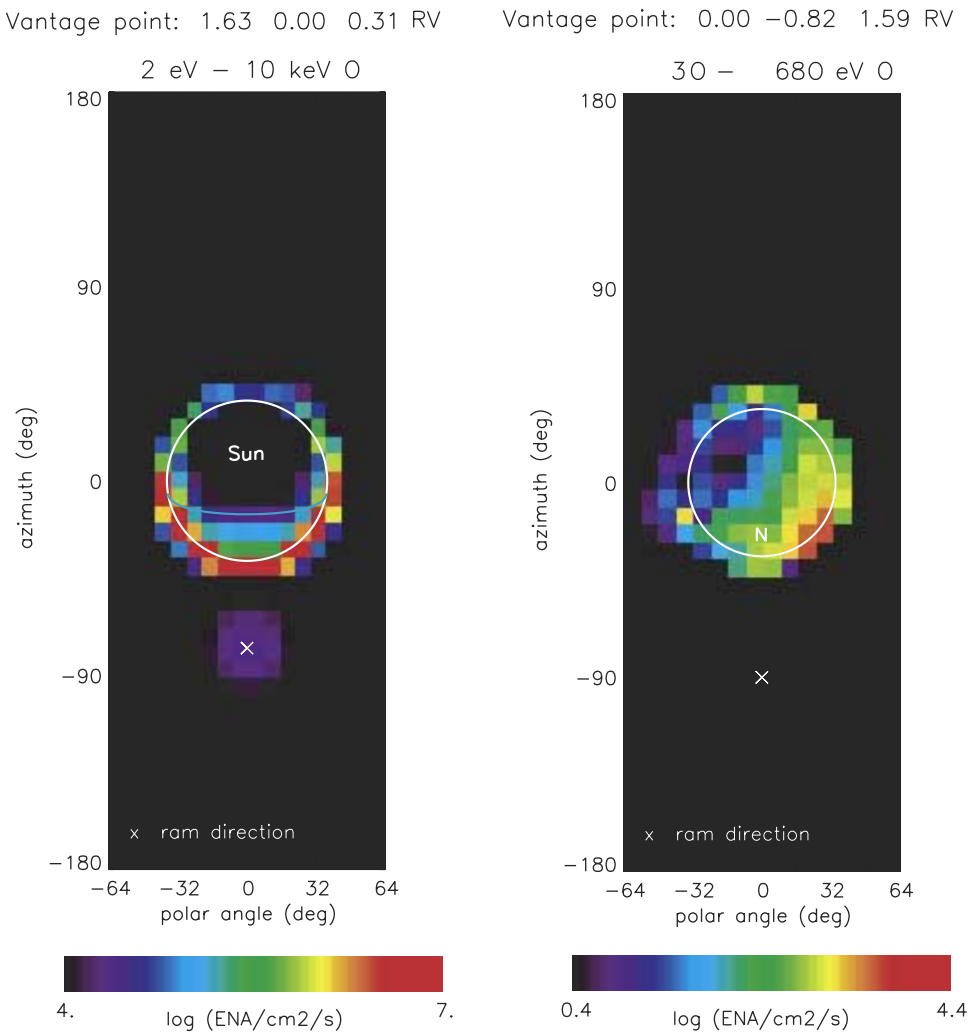

Figure 6. Same as Figure 5 except for oxygen ENA images.

away because their parent ions flow closely to and around the planet. Strongest escape rates are found at phi ~50° and 310°, corresponding to the wing-structure of the nightside O^+ density (Figure 4, lower-left panel). These peak emissions are confined to near the equator. The escape becomes more broad in latitude approaching midnight, where the magnetotail is thick. The slight dawn-dusk asymmetry in the escape rate is coming from small irregularities in the

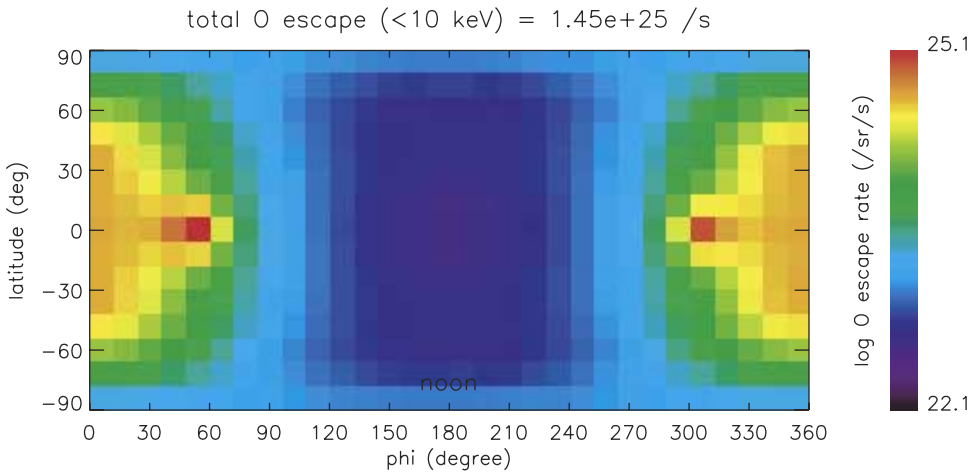

Figure 7. Simulated oxygen escape rate due to charge exchange processes. 180° phi corresponds to noon.

MHD results. The total oxygen escape rate estimated is $\sim 1.5 \times 10^{25}$ s^{-1}. This rate is thought to represent a lower limit on the escape rate of oxygen because the MHD model used here does not account for finite gyroradius oxygen pickup and thermalization processes which will greatly increase O^+ heating and subsequent escape of O produced by charge exchange, as occurs at the Earth owing to electrodynamic coupling between the solar wind and ionosphere in the auroral regions.

5. Discussions and Summary

[14] Strong terrestrial low energy neutral atom emissions were seen by the IMAGE LENA imager, coming from the subsolar magnetosheath during the great storm on 31 March 2001. These enhancements are produced when high solar wind pressure pushes the magnetosheath into the outer geocoronal hydrogen population. Similar magnetosheath emissions were also found during other storms. ENA images thus provide information about how the magnetosphere responds to the solar wind driver and the shape of the magnetosheath as it penetrates into the polar cusps. With further data analysis and modeling efforts, an algorithm can be established to infer the location and shape of the magnetopause using LENA data.

[15] Motivated by the terrestrial observations, we have carried out the first ENA simulation on Venus and have shown detectable high levels of ENA emissions from the planet. While sheath emissions at Earth are seen primarily during periods of high solar wind pressure, sheath emission at Venus is prominent even during nominal solar wind conditions. The O ENA flux on Venus is on the order of 10^7 ENA/cm^2/s, which is comparable with emission levels observed from the auroral zone at Earth but spread over large areas of the planet. Therefore the neutral atom imaging technique can be applied to study solar wind-Venus interactions and how the solar wind controls the shape of the bow shock, magnetosheath, and ionopause. One by-product from the ENA images will be to extract the in situ neutral temperature and density from the ram signals.

[16] We have calculated the oxygen escape rate due to charge exchange reactions between energetic ionospheric O^+ ions and neutral atoms in Venus exosphere. The total escape rate is $\sim 1.5 \times 10^{25}$ s^{-1}, which is 3 times the estimated value on Mars [*Barabash et al.*, 2002]. However, the MHD model and the simulations shown here do not consider the gyro-motion and nonadiabatic acceleration of O^+ ions, so the actual O^+ escape rate should be substantially higher. To make a better prediction, a particle trajectory study must be performed.

[17] In summary, from the simulations we have presented here, we found:

[18] 1. Neutral atom imaging is a new and useful tool for studying the solar wind interaction with the terrestrial magnetosphere. Locations of the magnetopause and cusps can be deduced from neutral atom images during events with elevated solar wind pressure.

[19] 2. A simulation study has shown significant low-energy (from zero to a few keV) neutral atom emissions from Venus.

[20] 3. Venus magnetosheath emissions have similar features and comparable intensity as those from the Earth during extreme solar wind condition.

[21] 4. Low-energy neutral O images from Venus can be used to probe the location and dynamics of the ionopause and the escape rates of escaping atmospheric atoms.

[22] 5. The estimated total O escape rate from Venus is 1.5×10^{25} s^{-1}.

[23] **Acknowledgments.** The MHD output for the 31 March 2001 event was provided by the Community Coordinated Modeling Center. The ACE data on the same day is downloaded from the ACE home page at http://www.srl.caltech.edu/ACE. We thank Gordon Chin for suggesting the Venus ENA calculation. We are grateful to Andrew Nagy and Thomas Cravens for many useful discussions. This work is supported partly by IMAGE mission under UPN 370-28-20.

[24] Lou-Chuang Lee thanks Richard L. Rairden and Bruce Tsurutani for their assistance in evaluating this paper.

References

Barabash, S., M. Holmstrom, A. Lukyanov, and E. Kallio (2002), Energetic neutral atoms at Mars: 4. Imaging of planetary oxygen, *J. Geophys. Res.*, *107*(A10), 1280, doi:10.1029/2001JA000326.

Burch, J. L. (2000), IMAGE mission overview, *Space Sci. Rev.*, *91*, 1–14.

Colin, L., and D. M. Hunten (1977), Pioneer-Venus experiment descriptions, *Space Sci. Rev.*, *20*, 451–525.

Collier, M. R., et al. (2001), Observations of neutral atoms from the solar wind, *J. Geophys. Res.*, *106*, 24,893–24,906.

Collier, M. R., T. E. Moore, D. Simpson, A. Roberts, A. Szabo, S. Fuselier, P. Wurz, M. A. Lee, and B. T. Tsurutani (2003), An unexplained 10°–40° shift in the location of some diverse neutral atom data at 1 AU, *Adv. Space Res.*, in press.

Cravens, T. E., T. I. Gombosi, and A. F. Nagy (1980), Hot hydrogen in the exosphere of Venus, *Nature*, *283*, 178–180.

Dunne, J. A. (1974), Mariner 10 Venus encounter, *Science*, *183*, 1289–1291.

Fuselier, S. A., H. L. Collin, A. G. Ghielmetti, S. E. Claflin, T. E. Moore, M. R. Collier, H. Frey, and S. B. Mende (2002), Localized ion outflow in response to a solar wind pressure pulse, *J. Geophys. Res.*, *107*(A8), 1203, doi:10.1029/2001JA000297.

Groth, C. P. T., D. L. Zeeuw, T. I. Gombosi, and K. G. Powell (2000), Global three-dimensional MHD simulation of a space weather event: CME formation, interplanetary propagation, and interaction with the magnetosphere, *J. Geophys. Res.*, *105*, 25,053–25,078.

Jastrow, R., and S. I. Rasool (1969), *The Venus Atmosphere*, Gordon and Breach, New York.

Keating, G. M., et al. (1985), Models of Venus neutral upper atmosphere: Structure and composition, *Adv. Space Res.*, *5*, 117–171.

Moore, T. E., et al. (2000), The low-energy neutral atom imager for IMAGE, *Space Sci. Rev.*, *91*, 155–195.

Moore, T. E., M. R. Collier, M.-C. Fok, S. A. Fuselier, H. Khan, W. Lennartsson, D. G. Simpson, G. R. Wilson, and M. O. Chandler (2003), Heliosphere-geosphere interactions using low energy neutral atom imaging, *Space Sci. Rev.*, in press.

Nagy, A. F., J. Kim, and T. E. Cravens (1990), Hot hydrogen and oxygen atoms in the upper atmospheres of Venus and Mars, *Ann. Geophys.*, *8*, 251–256.

Phillips, J. L., and D. J. McComas (1991), The magnetosheath and magnetotail of Venus, *Space Sci. Rev.*, *55*, 1–80.

Rairden, R. L., L. A. Frank, and J. D. Craven (1986), Geocoronal imaging with Dynamics Explorer, *J. Geophys. Res.*, *91*, 13,613–13,630.

Tanaka, T., and K. Murawski (1997), Three-dimensional MHD simulation of the solar wind interaction with the ionosphere of Venus: Results of two-component reacting plasma simulation, *J. Geophys. Res.*, *102*, 19,805–19,821.

M. R. Collier, M.-C. Fok, and T. E. Moore, Laboratory for Extraterrestrial Physics, NASA Goddard Space Flight Center, Mail Code 692, Greenbelt, MD 20771, USA. (mcollier@pop600.gsfc.nasa.gov; mei-ching.h.fok@nasa.gov; thomas.e.moore@nasa.gov)

T. Tanaka, Department of Earth and Planetary Science, Kyushu University, 6-10-1 Hakozaki, Higashi-ku, Fukuoka 8-12-8581, Japan. (tatanaka@geo.kyushu-u.ac.jp)